AIP | Journal of Applied Physics

Influence of the magnetization damping on dynamic hysteresis loops in single domain particles

Gabriel T. Landi

Citation: J. Appl. Phys. **111**, 043901 (2012); doi: 10.1063/1.3684629
View online: http://dx.doi.org/10.1063/1.3684629
View Table of Contents: http://jap.aip.org/resource/1/JAPIAU/v111/i4
Published by the American Institute of Physics.

Influence of the magnetization damping on dynamic hysteresis loops in single domain particles

Gabriel T. Landi[a)]
Instituto de Física da Universidade de São Paulo, 05314-970 São Paulo, Brazil

(Received 23 September 2011; accepted 11 January 2012; published online 16 February 2012)

This article reports on the influence of the magnetization damping on dynamic hysteresis loops in single-domain particles with uniaxial anisotropy. The approach is based on the Néel–Brown theory and the hierarchy of differential recurrence relations, which follow from averaging over the realizations of the stochastic Landau–Lifshitz equation. A new method of solution is proposed, where the resulting system of differential equations is solved directly using optimized algorithms to explore its sparsity. All parameters involved in uniaxial systems are treated in detail, with particular attention given to the frequency dependence. It is shown that in the ferromagnetic resonance region, novel phenomena are observed for even moderately low values of the damping. The hysteresis loops assume remarkably unusual shapes, which are also followed by a pronounced reduction of their heights. Also demonstrated is that these features remain for randomly oriented ensembles and, moreover, are approximately independent of temperature and particle size.
 [doi:10.1063/1.3684629]

I. INTRODUCTION

Magnetic single-domain particles have been actively studied for several decades, motivated by persistent theoretical and experimental advances and novel potential applications. This remains true nowadays, for instance in magnetic storage technologies[1] and magneto-hyperthermia treatments.[2] The most intensively studied effect present in these materials is their enhanced sensitivity to thermal fluctuations, a phenomenon known as superparamagnetism.[3–5] However, with fluctuations there is always dissipation. This *magnetization damping,* which has received considerable attention in recent years, also arises from the interaction of the constituent spins with the thermal bath. The microscopic degrees of freedom include, among others, nuclear spins, phonons, and conduction electrons, with the spin-orbit coupling seen as the key mechanism responsible for the energy transfer. Such complexity may be simplified, however, by introducing a phenomenological effective damping (α), as in the Landau-Lifshitz equation [see the upcoming Eq. (1)]. This allows the problem to be divided in two: understanding the origin of the damping and studying the effect it has on the magnetic properties of the system. This paper concerns the latter.

As for the former, the value of α has been determined for several materials, both experimentally[6–8] and through *ab initio* calculations.[9,10] In bulk ferromagnets and thin films it is known to be quite sensitive to the stoichiometry, crystallography, and temperature of the sample. For particulate systems, due to the reduced dimensionality, the particle's environment also plays a prominent role. For instance, they may be embedded in dielectric or metallic matrixes, either as solids or powders. Conversely, they may be dispersed in different solvents, with organic capping layers for protection or metallic shells tailored for specific applications. In most systems the damping is usually found to lie between $0.01 \lesssim \alpha \lesssim 1$, known as the low damping (LD) regime. In this interval the precessional modes of the magnetization are of considerable importance. Most notably, they enable the appearance of ferromagnetic resonance (FMR) in high frequency experiments. Another regime, frequently studied theoretically, is the intermediate-to-high damping (IHD) regime where $\alpha \geq 1$. Here these modes are assumed to be entirely suppressed, inhibiting any resonant responses.

Perhaps the most important problem in single-domain particles, both experimentally and theoretically, is that of *dynamic hysteresis* where an external harmonic field of arbitrary amplitude and frequency is applied. Its usefulness lies in the fact that within a single framework it is possible to transit between the linear and non-linear magnetic responses by modulating the field amplitude. In addition, there is no distinction between quasi-static or high-frequency loops enabling one to study any frequency desired. This problem was the subject of Refs. 11–15, all of which however, have not provided any consistent account of the influence of α. In particular, the effect that the FMR modes have on the hysteresis loops has thus far been entirely avoided. This was done either by assuming that the system was in the IHD regime or by limiting the frequency spectrum to sufficiently low frequencies.

If one combines the previous assertion that most real systems are in the LD regime with the fact that both of the aforementioned applications (and many others) employ frequencies precisely within the FMR range, it is possible to conclude that this problem is quite relevant and should not be ignored.

It is the primary goal of this paper to give a detailed investigation of the impact of the magnetization damping on dynamic hysteresis loops in single-domain particles with

[a)]Electronic mail: gtlandi@if.usp.br.

uniaxial anisotropy. The starting point is the Néel-Brown theory[16] in which the Landau-Lifshitz dynamical equation is augmented with a Gaussian white noise term to account for the interactions with the thermal bath. On averaging over the stochastic realizations it is possible to obtain an infinite hierarchy of differential recurrence relations describing the time evolution of the statistical moments of the magnetization. This in turn can be cast in the form of a system of coupled first-order linear ordinary differential equations (ODEs), which is straightforward to implement and solve numerically using any of the powerful algorithms available (here the SUNDIALS[17] library was employed). The sparsity of the system may also be exploited to significantly optimize the routines. Consequently, each loop takes on average only ~ 5 s to compute, which includes eliminating transient solutions that may survive for more than 100 periods. This is noteworthy given that the calculations involve no approximations whatsoever (except for those already implied by the theory itself). The author is also unaware of any papers using this method, with matrix continued fractions[18,19] (MCF) being the usual choice. As this paper will show, this approach is simple, fast, accurate, and hence competitive with any MCF method.

This paper considers the combined influence of all free parameters of uniaxial system. With the appropriate choice of coordinates this may be reduced to a total of five (explained in detail in Sec. II): the damping (α); the ratio of the anisotropy barrier and the thermal energy (σ); the field amplitude (h_0), its frequency (ω), and the angle it makes with the anisotropy axis (ψ). The influence of the damping is noticeable throughout the entire frequency spectrum. This study focuses, however, primarily on high frequencies near the FMR bands, where novel and unusual effects are observed. The hysteresis loops assume very exotic shapes, which are markedly sensitive to all parameters, an effect referred to as *resonant hysteresis* (RH). The situation of a transverse field encompasses several of the key aspects of RH loops. Therefore, a thorough account of this condition is first given in Sec. IV. Oblique angles are also discussed, focusing on the representative case of $\psi = 45°$ (Sec. V). In Sec. VI it is shown that RH loops in randomly oriented ensembles (mimicking real samples) retain most of the important features of their orientally textured counterparts. Moreover, they are also approximately independent of temperature, remaining visible even in the superparamagnetic regime. These assertions combined indicate that RH is, in fact, prone to experimental investigation.

II. NÉEL-BROWN THEORY

The magnetic Langevin equation corresponds to the Landau-Lifshitz equation for a magnetic dipole, augmented with a Gaussian white noise *thermal field* $\boldsymbol{H}_{\rm th}$ whose Cartesian coordinates satisfy the statistical properties: $\langle H^i_{\rm th}(t)\rangle = 0$ and $\langle H^i_{\rm th}(t) H^i_{\rm th}(s)\rangle = 2(k_B T\eta/v)\delta_{i,j}\delta(t-s)$. Here v is the particle's volume, T is the temperature, k_B is Boltzmann's constant, and η is the dimensionless damping parameter. The Kronecker and Dirac deltas indicate that the thermal field is both spatially and temporally uncorrelated. Whence, the magnetic Langevin equation (or, similarly, the Stochastic Landau-Lifshitz equation) is

$$\left(1+\alpha^2\right)\frac{d\boldsymbol{M}}{dt} = -\gamma_0 \boldsymbol{M}\times(\boldsymbol{H}_e + \boldsymbol{H}_{\rm th}) - \frac{\alpha\gamma_0}{M_s}\boldsymbol{M}\times[\boldsymbol{M}\times(\boldsymbol{H}_e+\boldsymbol{H}_{\rm th})], \tag{1}$$

where γ_0 is the electron's gyromagnetic ratio and $\alpha = \gamma_0 \eta M_s$ is what shall effectively be used as the damping parameter. The effective field $\boldsymbol{H}_{\rm e}$ is obtained from the gradient of the free energy which reads

$$E = -\boldsymbol{M}\cdot\boldsymbol{H} - \frac{K}{M_s^2}(\boldsymbol{M}\cdot\mathbf{u})^2, \tag{2}$$

where $\boldsymbol{H}$ is the externally applied field, K is the anisotropy constant, M_s is the saturation magnetization and $\mathbf{u} \equiv \hat{\mathbf{e}}_z$ is the unit vector in the direction of the anisotropy axis. Thus,

$$\boldsymbol{H}_e = -\frac{\partial E}{\partial \boldsymbol{M}} = \boldsymbol{H} + \frac{2K}{M_s^2}(\boldsymbol{M}\cdot\mathbf{u})\mathbf{u}. \tag{3}$$

The unit vector $\mathbf{m} = \mathbf{M}/M_s$ is used to describe the magnetization and $\mathbf{h} = \boldsymbol{H}/H_A$ for the external field, where $H_A = 2K/M_s$ is the maximum coercive field available in the context of the model of Stoner and Wolfarth.[20] The Langevin equation then takes the following simple form:

$$\left(1+\alpha^2\right)\tau_0\frac{\mathrm{d}m}{\mathrm{d}t} = -m\times(\mathbf{h}_{\rm e}+\mathbf{h}_{th}) - \alpha m\times[\mathbf{m}\times(\mathbf{h}_{\rm e}+\mathbf{h}_{\rm th})], \tag{4}$$

where $\tau_0 = (\gamma_0 H_A)^{-1}$. Note that this definition of τ_0 differs from what is sometimes used in the literature, namely $\tau_0' = (1+\alpha^2)(\alpha\gamma_0 H_A)^{-1}$. The obvious reason for this choice is that in investigating the influence of α it is important that the time scale be independent of it. The effective field (3) becomes

$$\mathbf{h}_{\rm e} = \mathbf{h} + m_z\hat{e}_z \tag{5}$$

and the thermal field may now be written very simply as

$$\left\langle h^i_{\rm th}(t)\right\rangle = 0, \quad \left\langle h^i_{\rm th}(t)h^i_{\rm th}(s)\right\rangle = \frac{\alpha}{\sigma}\delta_{i,j}\delta(t-s), \tag{6}$$

where $\sigma = Kv/k_B T$ is what shall be used as a measure of inverse temperature.

The magnetic field is assumed to be harmonic, with amplitude h_0 and frequency ω (given in units of τ_0), which makes an angle ψ with the z axis:

$$\mathbf{h} = h_0(\gamma_x\hat{\mathbf{e}}_x + \gamma_z\hat{\mathbf{e}}_z)\cos\omega t, \tag{7}$$

where $\gamma_x = \sin\psi$ and $\gamma_z = \cos\psi$. Thus, the problem is completely determined by the following five parameters: α, σ, h_0, ω, and ψ; all important and all investigated in this paper.

In passing it is noted that when $\psi = 0$, axial symmetry is preserved so that, except for a multiplicative factor, the hysteresis loops are independent of α. Thus, this problem will not be treated in this paper (see, for instance, Refs. 13–15).

III. METHODS OF SOLUTION

The development of the hierarchy of differential recurrence relations is performed in spherical coordinates where $m_z = \cos\theta$ and $m_x + im_y = \sin\theta e^{i\phi}$. The statistical moments may then be represented in terms of spherical harmonics defined as[21]

$$Y_{l,m}(\theta,\phi) = \sqrt{\frac{2l+1}{4\pi}\frac{(l-m)!}{(l+m)!}}P_l^m(\cos\theta)e^{im\phi}, \tag{8}$$

with $l = 0, 1, 2, \ldots$ and $-l \leq m \leq l$. Here P_l^m are the associated Legendre functions.

Let $f(\mathbf{m})$ be an arbitrary function of the random set $\{m_x, m_y, m_z\}$. On performing an initial average over sharp initial conditions it is possible to derive[18] the following equation for the time evolution of f:

$$(1+\alpha^2)\tau_0\frac{\mathrm{d}f}{\mathrm{d}t} = -[\mathbf{m}\times\mathbf{h} + \alpha\mathbf{m}\times(\mathbf{m}\times\mathbf{h})]\cdot\frac{\partial f}{\partial\mathbf{m}} + \frac{\alpha}{2\sigma}\left(\mathbf{m}\times\frac{\partial}{\partial\mathbf{m}}\right)^2 f. \tag{9}$$

The last term follows from the noise-induced drift and can be identified with the angular momentum operator $-\hat{L}^2$. Thus, taking $f(\mathbf{m}) = Y_{l,m}(\theta, \phi)$ the result is $\hat{L}^2 Y_{l,m} = l(l+1)Y_{l,m}$. The first term in Eq. (9) will, in general, contain products of spherical harmonics, which must be written exclusively as linear combinations of these functions. The procedure, albeit straightforward in essence, involves some algebraic manipulations. The transformations can be accomplished by means of three formulas, which are given in Appendix A, together with further details on how to affect the calculation. Once it is done, another ensemble average must be taken over $W(\mathbf{m}; t)$ (denoted by angular brackets). The final result is

$$\begin{aligned}
\frac{(1+\alpha^2)}{\alpha}\tau_0\frac{\mathrm{d}\langle Y_{l,m}\rangle}{\mathrm{d}t} = {} & \left[\frac{l(l+1)-3m^2}{(2l-1)(2l+3)} + \frac{imh_0\gamma_z}{\alpha} - \frac{l(l+1)}{2\sigma}\right]\langle Y_{l,m}\rangle + \frac{l+1}{2l-1}\sqrt{\frac{(l^2-m^2)\left[(l-1)^2-m^2\right]}{(2l+1)(2l-3)}}\langle Y_{l-2,m}\rangle \\
& - \frac{l}{2l+3}\sqrt{\frac{\left[(l+1)^2-m^2\right]\left[(l+2)^2-m^2\right]}{(2l+1)(2l+5)}}\langle Y_{l+2m}\rangle + \left(h_0\gamma_z(l+1) + \frac{im}{\alpha}\right)\sqrt{\frac{l^2-m^2}{4l^2-1}}\langle Y_{l-1,m}\rangle \\
& - \left(h_0\gamma_z - \frac{im}{\alpha}\right)\sqrt{\frac{(l+1)^2-m^2}{(2l+1)(2l+3)}}\langle Y_{l+1,m}\rangle + \frac{h_0\gamma_x}{2}\left\{(l+1)\sqrt{\frac{(l-m-1)(l-m)}{(2l-1)(2l+1)}}\langle Y_{l-1,m+1}\rangle\right. \\
& - (l+1)\sqrt{\frac{(l+m-1)(l+m)}{(2l-1)(2l+1)}}\langle Y_{l-1,m-1}\rangle + l\sqrt{\frac{(l+m+1)(l+m+2)}{(2l+1)(2l+3)}}\langle Y_{l+1,m+1}\rangle \\
& \left. - l\sqrt{\frac{(l-m+1)(l-m+2)}{(2l+1)(2l+3)}}\langle Y_{l+1,m-1}\rangle + \frac{i}{\alpha}\sqrt{(l+m+1)(l-m)}\langle Y_{l,m+1}\rangle + \frac{i}{\alpha}\sqrt{(l-m+1)(l+m)}\langle Y_{l,m11}\rangle\right\}.
\end{aligned} \tag{10}$$

This equation was first obtained by Coffey *et al.*[22] and is discussed in detail in Ref. 18. All terms involving α in Eq. (10) are followed by the imaginary unit and hence the equations must be separately solved for the $\langle\mathrm{Re}(Y_{l,m})\rangle$ and $\langle\mathrm{Im}(Y_{l,m})\rangle$. Negative values of the index m are avoided by means of the formulas $\mathrm{Re}(Y_{l,-m}) = (-1)^m\mathrm{Re}(Y_{l,m})$ and $\mathrm{Im}(Y_{l,-m}) = (-1)^{m+1}\mathrm{Im}(Y_{l,m})$.

The next step is to truncate this infinite hierarchy at some point, e.g., N, and write it as a system of ODEs,

$$\dot{\mathbb{X}} = \mathscr{F}\mathbb{X} + \mathbb{U}, \tag{11}$$

where $\mathbb{X}$ and $\mathbb{U}$ are column vectors of length N and $\mathscr{F}$ is an $N\times N$ matrix. The value of N can be easily determined by inspection. It is known that it must be increased with increasing σ and decreasing α. This research have found that, in all situations here studied, it sufficed to set $N \sim 10^3$. For safety, $N = 1400$ was used. It follows that, in this case, less than 1% of the terms in $\mathscr{F}$ are non-zero, thus emphasizing the importance of adequately benefiting from its sparsity. Also note that both $\mathscr{F}$ and $\mathbb{U}$ now depend explicitly on time through $\mathbf{h}$ [Eq. (7)].

The quantity of interest is the projection of the magnetization onto the field direction, which is denoted simply as m_h,

$$\begin{aligned}
m_h(t) &= \gamma_z\langle m_z\rangle(t) + \gamma_x\langle m_x\rangle(t) \\
&= \sqrt{\frac{4\pi}{3}}\left[\gamma_z\langle Y_{1,0}\rangle(t) - \sqrt{2}\gamma_x\langle\mathrm{Re}(Y_{1,1})\rangle(t)\right].
\end{aligned} \tag{12}$$

The results may be cast in the form of average trajectories $(m_h(t))$ or, by means of a parametric plot, as hysteresis loops $(m_h(h))$.

Equation (11) corresponds to a system of coupled first-order linear ODEs, which may be solved directly by standard methods. The SUNDIALS[17] library was opted for, which is not only remarkably fast but also conveniently handles two important features of this system. First, the fact that the equations are stiff, which originate from the vastly different rates of change of the statistical moments. Thus, backward differentiation formulas were used. Secondly, even though $\mathscr{F}$ is sparse, it is not tightly banded. Thence, Krylov iterative linear solvers are much more efficient in treating the system's Jacobian than banded Newton methods.

The hysteresis loops must be independent of initial conditions so that transients need to be completely eliminated. The simplest (and safest) way to do this is to start with equilibrium in the absence of any external field and then proceed with the integration, computing one period at a time and testing weather the loop has changed up to some tolerance when compared to the previous period. One may also gain additional efficiency if curves for different frequencies are computed sequentially. This way the final solution vector of the previous computation may be used as the initial condition for the current one, hence partially skipping the transients. For low frequencies, two periods usually suffice, whereas on the other extreme up to 100 periods may be required. But, as the periods are shorter the net computing time remains roughly the same. In order to meet the prescribed error tolerances the number of steps is automatically adjusted and hence the computation time varies with the parameters. The average loop takes $\sim$5 s on a simple desktop computer. For low σ, low h_0 or high α, times as small as $\sim$1 s are observed. Conversely, for $\alpha = 0.05$ they rise to $\sim$30 s and may as well surpass $\sim$200 s when $\alpha = 0.01$, a situation that this study has therefore opted to avoid. Note, however, that even such long times are still negligibly small compared to other methods such as the Stochastic Landau-Lifshitz (SLL) (see the following).

In order to quantify some properties of the hysteresis loops the following useful parameters are defined. The coercive field (h_c) is such that $m_h(h_c) \equiv 0$ with $0 \le h_c \le h_0$. Much more interesting is the coercive time (t_c) defined so that $m_h(t_c) \equiv 0$, but with $\pi/2 \le t_c \le 3\pi/2$; i.e., independent of ω. If $t_c = \pi/2$ there is no hysteresis, whereas if $t_c > \pi$ the reversal time has surpassed the extrema of cos ωt and the loops become asymmetrical. This region is referred to as the asymmetric regime and the frequency where $t_c = \pi$ as the asymmetry threshold frequency (ATF). It is also convenient to define the average susceptibility per cycle as

$$\chi = \chi' - i\chi'' = \frac{\omega}{\pi h_0}\int_0^{2\pi/\omega} m_h(t) e^{i\omega t} dt, \tag{13}$$

where χ' is related to the average phase-lag between m_h and h, whereas χ'' is proportional to the energy dissipated per cycle (the loop area in this notation is $A = \pi h_0^2 \chi''$). With this definition, if $h_0 \ll 1$, the susceptibility should tend to the linear response result

$$m_h(t) = h_0(\chi' \cos\omega t + \chi'' \sin\omega t). \tag{14}$$

As will become evident $t_c = \pi$ necessarily implies $\chi' = 0$, which may therefore also be taken as a signature of the ATF. In passing, this frequency roughly coincides with the linear response resonance frequency, $\omega_R \simeq \gamma_0 H_A$ (i.e., $\omega_R \tau_0 \simeq 1$). In problems involving harmonic fields, it is customary to expand the susceptibility in a Fourier series[22–25] and thus analyze each component separately. Therefore, it is worth noting that due to the orthogonality of the harmonic functions, the definition here[13] agrees with the first component of this Fourier series.

As an auxiliary method this research directly solved the stochastic differential equation (4) using Heun's scheme.[26,27] This will be referred to as the SLL method (which stands for Stochastic Landau-Lifshitz). The average was done of a total of 10^4 realizations over 80 periods of the external field; the first 40 were discarded and a second average over the remaining was then carried. The entirely different nature of both methods should serve as a convenient check of the validity of these results.

Finally, also performed were calculations using linear response theory (LRT), whose starting point is also Eq. (11). It allows inexpensive computation of $\chi(\omega)$ and serves as a useful benchmark. Details of the procedure are given in Appendix B. See also Ref. 18 and references therein.

IV. RESPONSE TO A TRANSVERSE FIELD

The case where $\psi = 90°$ is a peculiar one as the external field does not introduce any asymmetries in the energyscape of Eq. (2). The ensemble remains with roughly half of its spins in each hemisphere ($m_z \gtrless 0$) except that now $\langle m_x \rangle \neq 0$. This means that only precessional modes are excited and consequently, any hysteresis observed cannot originate from overbarrier processes. Indeed, they must arise solely from the gyromagnetic response, viz. the restriction over the magnetic moment to precess exclusively on the unit sphere.

Hysteresis loops for different values of ω and α are shown in Fig. 1 for $h_0 = 1$ and $\sigma = 10$ (which may be taken as "moderately cold"). The value $\alpha = 1$, as is known from the LRT, is already in the IHD regime. The corresponding loops thus follow a simpler behavior, becoming increasingly shorter and wider as ω increases. They finally become quasi-elliptical by the time $\omega\tau_0 = 1.5$, with the major axis approaching the abscissa. Conversely, the LD curves ($\alpha < 1$) show a drastically different response. The loops assume a variety of unusual shapes and between $\omega\tau_0 = 0.4$ and 0.6 the apex of the curves get bent up (by apex it is meant the point where $h = 1$; conversely, the point where $h = -1$ gets bent down). Finally, when $\omega\tau_0 = 1.5$ the loops become quasi-elliptical and out-of-phase with the external field, meaning the ATF has been supassed.

In order to gain a more thorough insight into the transition that takes place between $\omega\tau_0 = 0.4$ and 0.6, presented in Fig. 2 are trajectories $m_h(t)$, together with their corresponding loops, when $\alpha = 0.02$. The external field is depicted in dashed, normalized to fit the plot.

Attention is also called to the fact that in order to properly visualize the curves the vertical scale had to be expanded. The importance of the apex becomes clear from the $m_h(t)$ curves in the sense that they correspond to peaks that appear precisely at the extrema of h. As ω approaches the resonance region they become increasingly more pronounced but, concurrently, the rest of the loops become

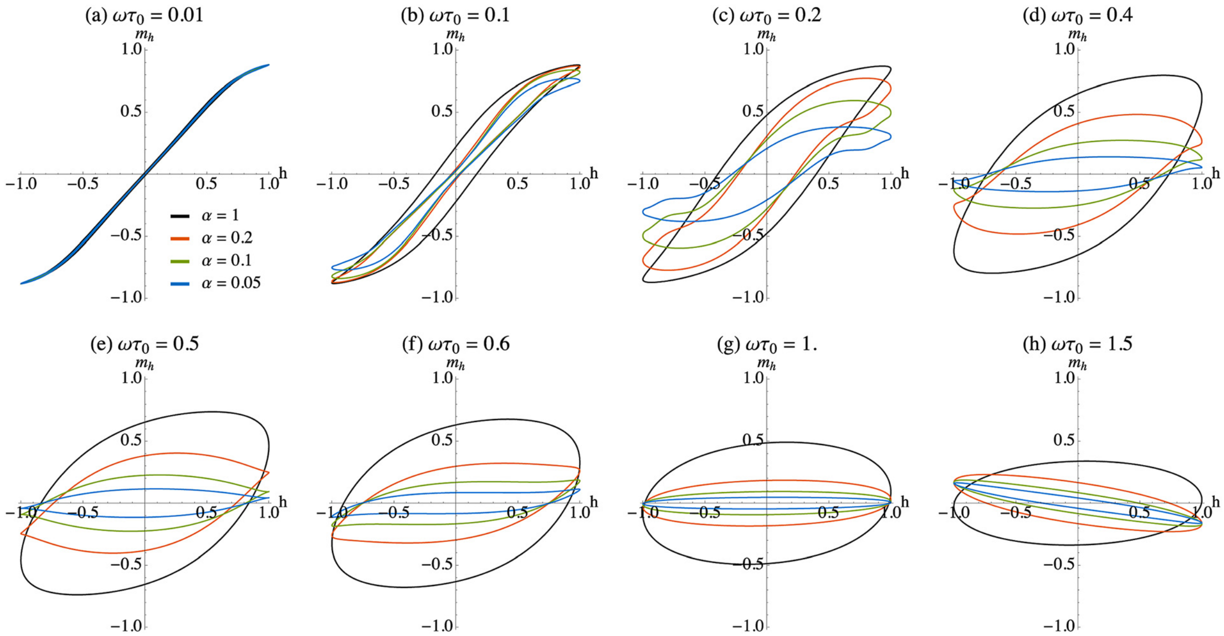

FIG. 1. (Color online) Hysteresis loops for different values of α and ω with fixed $\sigma = 10$, $h_0 = 1$, and $\psi = 90°$.

suppressed. Consequently, it eventually comes a point where the trajectory shifts in phase with the field. While not shown, for even higher frequencies the apex is also eventually suppressed, and the phase lag starts to increase once again until finally surpassing $\pi/2$ at the ATF. Given the atypical shapes of the loops it seems natural to query the correctness of the results. To settle this, Fig. 2 also presents hysteresis loops calculated using the SLL approach. The agreement, as can be seen, is irrefutable. Any discrepancies arise from the statistical nature of the latter and can be made arbitrarily small by increasing the number of realizations computed.

Another important effect observed in Fig. 1 regards the sensitive dependence of the loop heights with α. An abrupt change is observed between $\omega\tau_0 = 0.1$ and 0.2, which gradually continues as ω is increased further; when $\omega\tau_0 = 0.4$ there is an almost fivefold difference between $\alpha = 1$ and $\alpha = 0.05$. This behavior follows immediately from the fact that the lower the damping the longer the magnetization takes to adjust itself to the external field. Hence, the number of spins crossing the $m_x = 0$ plane also becomes considerably smaller. It is important to stress that, on average, the height is a direct measure of the number of spins that are able to follow the external field. Besides the temperature, this number is also suppressed by the gyromagnetic response, as seen in the IHD curves ($\alpha = 1$). However, the dependence with α is a complementary effect and takes place at frequencies where the gyromagnetic response does not have a strong influence, $\omega\tau_0 = 0.4$ being a good example.

This paper now turns to a quantitative analysis in terms of the susceptibility and the coercive time, as presented in Fig. 3 for $\sigma = 10$. The linear χ', shown in the inset of Fig. 3(a), illustrates the FMR and serves as a useful guideline. It has a pronounced maxima followed by a negative minima, both of which increase considerably in magnitude as α is decreased. As one might expect from the nonlinearity of the problem, the behavior of χ' for $h_0 = 1$ differ dramatically from its linear counterpart. It shows no maxima, decaying from its quasi-static value until the ATF. Afterwards, all LD curves become negative and, interestingly, overlap entirely. This indicates that in this regime the

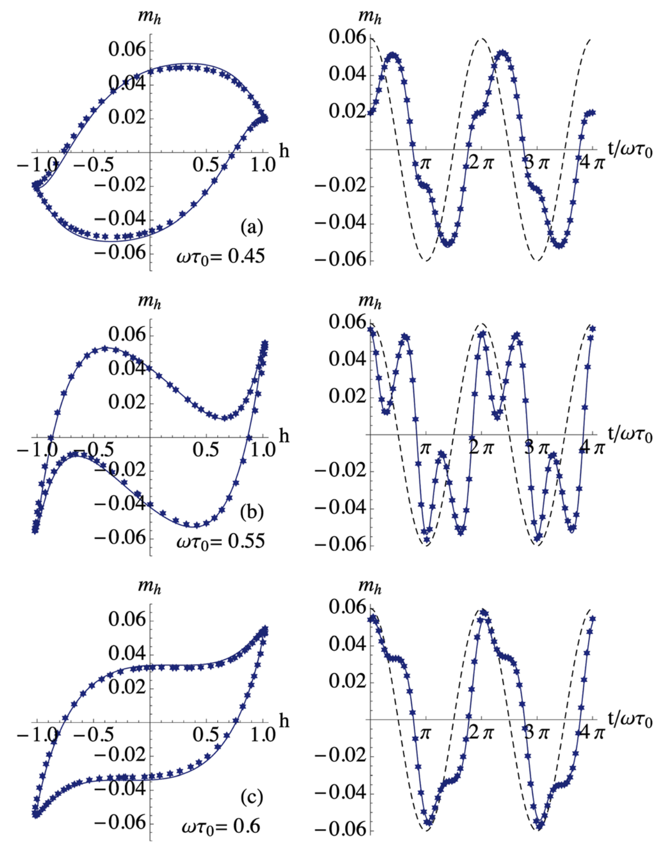

FIG. 2. (Color online) Hysteresis loops $m_h(h)$ (left) and corresponding trajectories $m_h(t)$ (right) for different values of ω with fixed $\alpha = 0.02$, $\sigma = 10$, $h_0 = 1$, and $\psi = 90°$. The magnetic field (cos ωt) is shown as a dashed line, also normalized to fit the graph. Asterisks were computed using the SLL method.

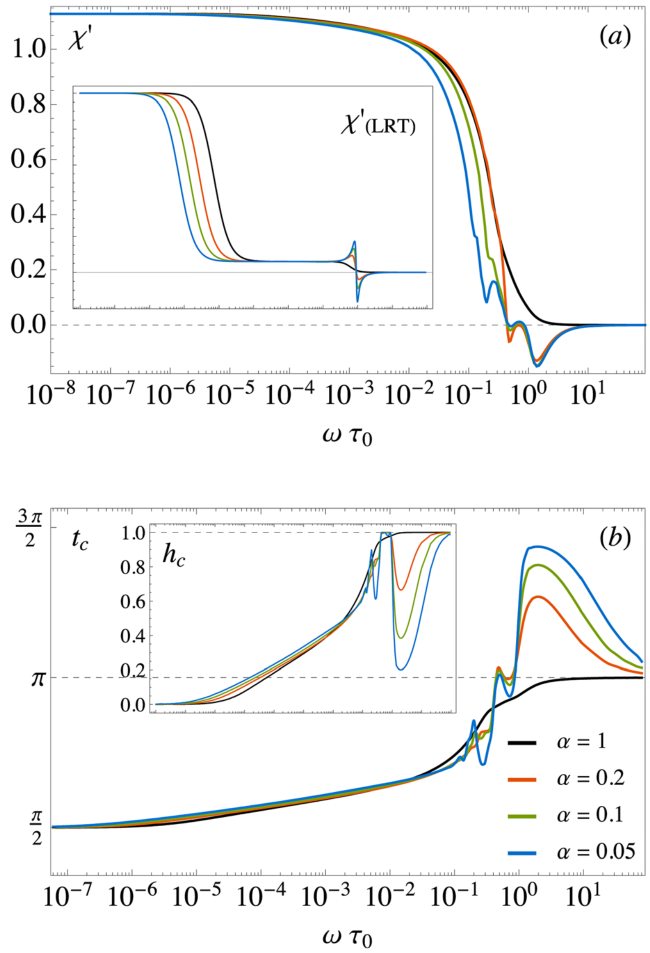

FIG. 3. (Color online) Parameters obtained from the hysteresis loops as a function of frequency, with fixed $\sigma = 10$, $h_0 = 1$, and $\psi = 90°$. (a) Real part of the average susceptibility, Eq. (13); (inset) LRT counterpart. (b) Coercive time; (inset) coercive field.

average phase-lag is independent of α, which is quite different from the linear response. The coercive time shown in Fig. 3(b) starts with $t_c = \pi/2$ (zero coercivity) and increases to $t_c = \pi$ as ω approaches the ATF. Similarly to χ', all LD curves enter the asymmetric region, first reaching a maxima which now increases with decreasing α, and then tending back toward $t_c \to \pi$ as $\omega \to \infty$. As a consequence of t_c surpassing π, even though the coercive field (inset) reaches unity near ω_R, it then falls significantly at the asymmetric region, reaching values as low as $h_c = 0.2$.

It is also possible to observe in Fig. 3 a "noisy" oscillatory behavior before ω_R. This, to emphasize, is by no means an artifact of the numerical procedure. In fact, it is an intrinsic property of the non-linearity of RH loops. Figure 2 may serve to further illustrate this point. Note, for instance, that the coercive field in Fig. 2(b) is simultaneously larger than those of Figs. 2(a) and 2(c), the same being true for the height. It is also worth mentioning that the oscillations remain for all other angles (cf. the upcoming Fig. 7). The noisiness, however, is peculiar of $\psi = 90°$, being a consequence of it is highly symmetric energyscape (i.e., the oscillations become smoother). Finally, note that similar results have been obtained by Mrabti *et.al.*,[23] which draw an interesting comparison between these oscillations and non-linear resonance phenomena occurring in soft springs. Indeed, a characteristic of the latter is the appearance of a second resonance peak at frequencies of $\sim\omega_R/2$, similarly to what is observed in Fig. 3.

Next, the temperature dependence focusing on the LD case $\alpha = 0.05$ is studied, as shown in Fig. 4. The vertical scale has once again been expanded in order to better visualize the results. Overall, increasing the temperature decreases the loop height and simultaneously makes some of the sharper features smoother. Notwithstanding, the RH remain clearly visible indicating that they are not restricted to low temperature conditions. In this image it is also possible to

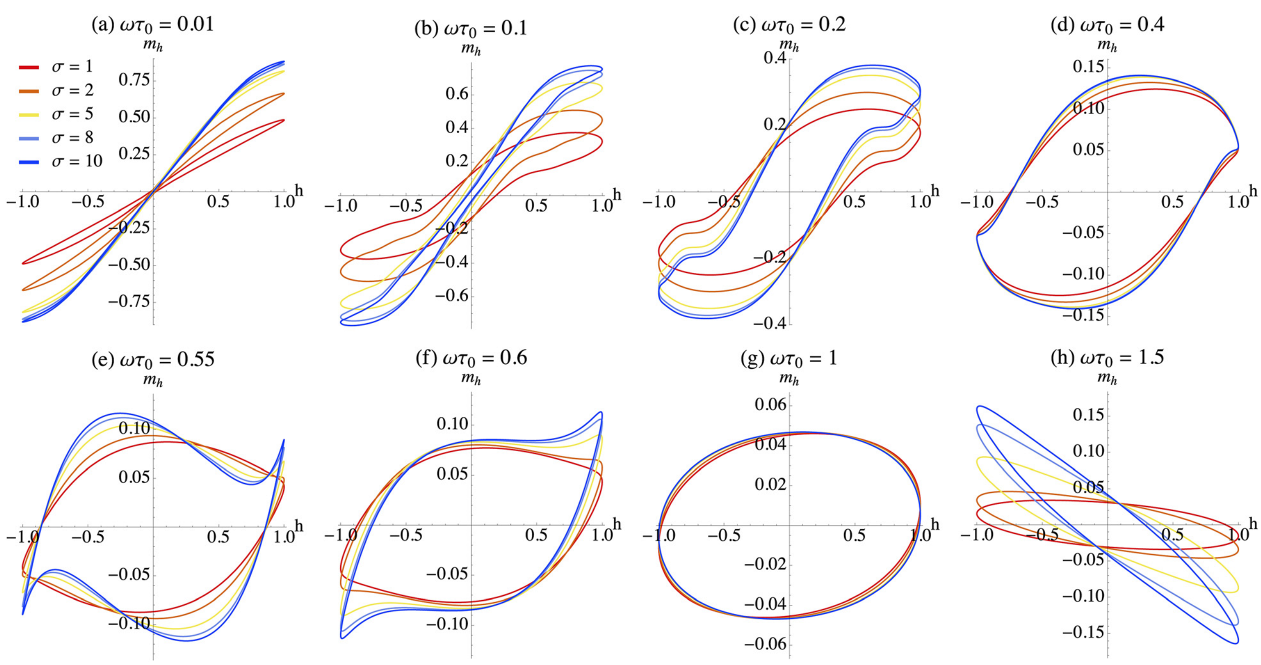

FIG. 4. (Color online) Temperature dependence ($\sigma \propto 1/T$) of the hysteresis loops for different values of ω with $\alpha = 0.05$, $h_0 = 1$, and $\psi = 90°$.

observe a quite remarkable phenomenon: As the frequency approaches the ATF [Figs. 4(d)–4(g)], the loops become approximately independent of temperature but, afterward, the usual dependence returns. This indicates that the resonant modes that are being excited are so intense—due to the strong external field—that the thermal fluctuations become practically innocuous. Also note that this is exclusive of the LD regime (cf. the upcoming Fig. 10). Another interesting effect, also exclusive of this regime, is that the loops become wider with increasing temperature, in contrast to the usual superparamagnetic behavior. Such result is peculiar of $\psi = 90°$ as no overbarrier processes are involved and shows that the damping has indeed a noticeable influence on the thermal response.

V. RESPONSE TO OBLIQUE FIELDS

Hysteresis loops for oblique fields contain both longitudinal and transverse relaxation mechanisms. Consequently, the FMR response gets superimposed by interwell and intrawell dynamical modes arising from the finite anisotropy barrier that the spins must now surmount. The former preponderate at the low frequency part of the spectrum where the external field is capable of reversing practically all spins during each half-cycle (the loops saturate). In this region α does not have a strong influence so that the average width of the loops is determined mainly by the competing effects of σ and ω. The intrawell modes, on the other hand, correspond to the motion near the bottom of the potential wells. They usually take place at higher frequencies where the gyromagnetic response time impedes the spins to overcome the energy barrier. However, in the LD regime this region usually coincides with the FMR bands, thus making the distinction between them not always entirely clear. In this section the focus is on the representative case of $\psi = 45°$. The temperature dependence, as found, is quite similar to what is observed in Fig. 4 and therefore was fixed once again $\sigma = 10$.

Figure 5 presents curves for different values of α and ω with $h_0 = 1$, $\sigma = 10$, and $\psi = 45°$. The interwell modes are clearly demonstrated in Figs. 5(a) and 5(b), where the area increases with ω, both situations being almost independent of α. More significant changes are first observed between $\omega\tau_0 = 0.01$ and 0.1, exactly as in Fig. 1. This is expected as most changes in this region should arise from transverse modes. However, these are now mixed with interwell and intrawell modes and consequently the curves become even more deformed, and their behavior even more unpredictable. There are two other similarities with the transverse case that are also clearly visible. The first is the rapid diminution of the loop heights that take place between $\omega\tau_0 = 0.1$ and 0.2, whereas the second is that after the ATF [Fig. 5(h)], the LD loops turn into asymmetrical quasi-ellipsoids. These results show that overbarrier processes are also strongly suppressed in low damping environments.

It is important to stress that the frequencies presented in Fig. 5 by no means exhaust the number of different shapes which appear over the range $0.1 \lesssim \omega\tau_0 \lesssim 1.0$. In fact, it is striking how abruptly the loops (and particularly their heights) may change over very small frequency intervals. To further illustrate this, Fig. 6 shows two loops for $\alpha = 0.02$ when $\omega\tau_0 = 0.26$ and 0.28. It can be seen that, even though the shape of the curves are somewhat similar, their heights nearly double from one to the other, from $\sim$0.11 to $\sim$0.19. Once again, the superimposed calculations using the SLL method serve as an independent check of the correctness of the results.

Now turn to χ' and t_c once again (Fig. 7). In the linear regime (inset) the interwell and FMR modes are clearly separated by several decades in frequency. This follows from the fact that the weak field is only capable of promoting spin reversals at very low frequencies, where it is assisted by the thermal fluctuations. When $h_0 = 1$ this is certainly not the

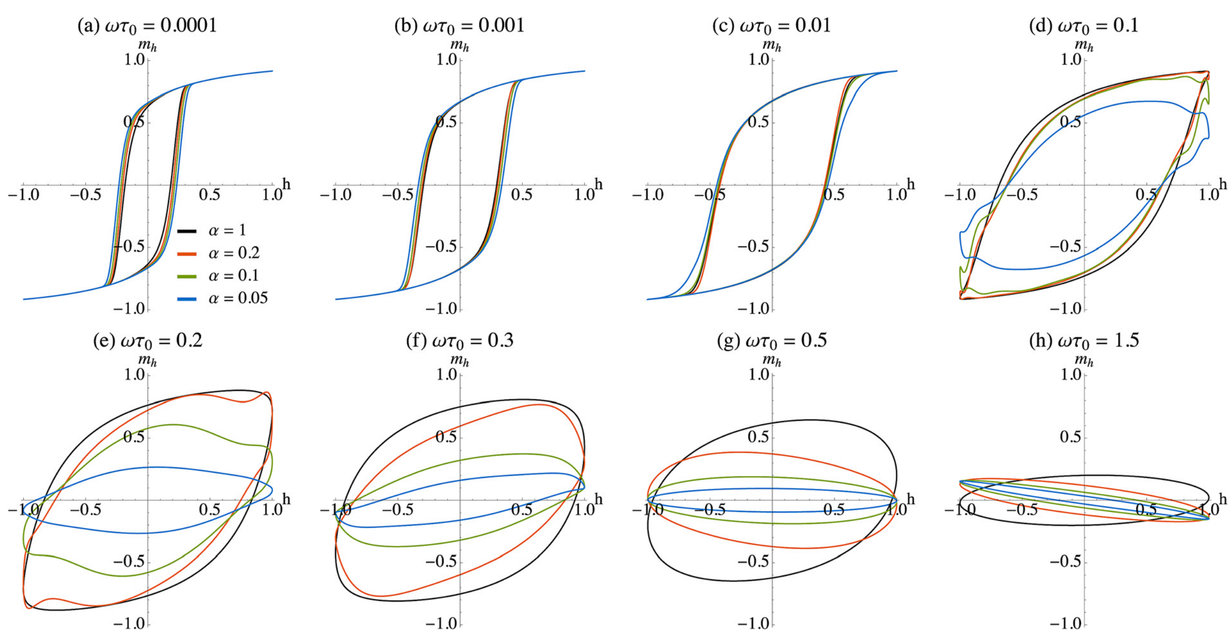

FIG. 5. (Color online) Hysteresis loops for different values of α and ω with fixed $\sigma = 10$, $h_0 = 1$, and $\psi = 45°$.

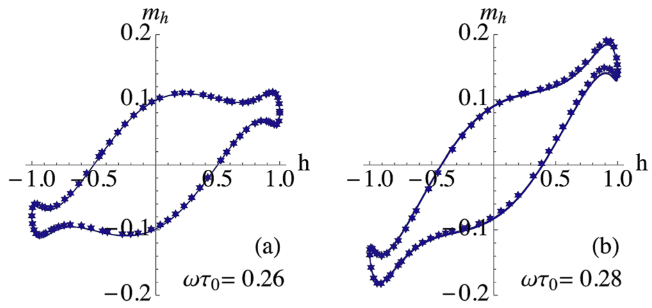

FIG. 6. (Color online) Hysteresis loops for $\alpha = 0.02$, $\sigma = 10$, $\psi = 45°$, and $h_0 = 1$. Asterisks correspond to the SLL method.

case and therefore χ' remains close to its quasi-static value up until $\omega\tau_0 \simeq 0.1$. Afterward it abruptly falls in a oscillatory and irregular fashion, becoming negative after the ATF. The coercive time in Fig. 7(b) first increases monotonically and slowly with ω, from $t_c = \pi/2$ when $\omega = 0$ to $t_c \sim 3\pi/4$ when $\omega\tau_0 \simeq 0.1$. It then enters the resonant regime, oscillating fiercely and eventually crossing the ATF near ω_R. There is a clear similarity in the asymmetric region, between Figs. 3 and 7. In particular, χ' also becomes independent of α when in the LD regime.

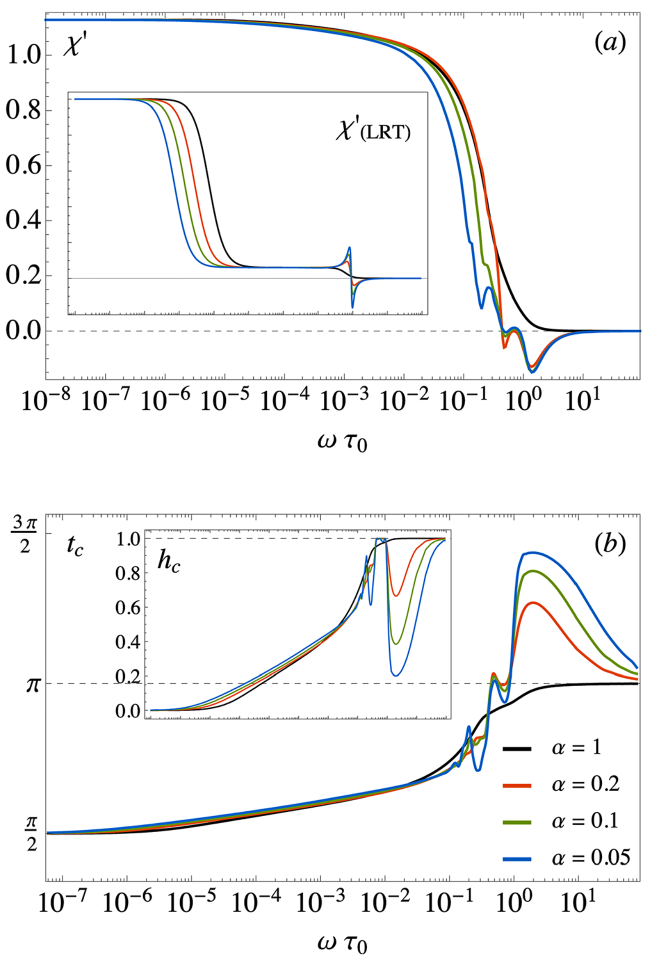

FIG. 7. (Color online) Parameters obtained from the hysteresis loops as a function of frequency, with fixed $\sigma = 10$, $h_0 = 1$, and $\psi = 45°$. (a) Real part of the average susceptibility, Eq. (13); (inset) LRT counterpart. (b) Coercive time; (inset) coercive field.

A noticeable phenomena appear in the oscillations, which happen before the ATF in Fig. 7. Not only are they smoother than when $\psi = 90°$, as already anticipated, but in the second one the curves briefly surpass the asymmetry threshold during a narrow frequency interval before proceeding toward the actual ATF. To explain these results recall some properties of longitudinal ($\psi = 0$) hysteresis loops discussed in Refs. 13 and 14. During each cycle the time window that the external field has to promote spins from (for instance) $m_z > 0$ to $m_z < 0$ is $\pi/(2\omega) \le t \le 3\pi/(2\omega)$, corresponding to the region where $h < 0$. In the model of Stoner and Wolfarth all spins flip at $t = \pi/\omega$ and, at finite temperatures, this usually occurs at earlier times since the thermal fluctuations facilitate the process. However, albeit unlikely, it is possible that the reversal occurs after $t = \pi/\omega$ as a consequence of the combined influence of the gyromagnetic and thermal responses. Thence the observed reaction is lagged and the corresponding loops asymmetrical. This effect, also referred to as *noise induced switching* in some contexts,[28] only remains during a narrow frequency interval, after which intrawell modes become dominant. It is also entirely independent of any FMR modes, occurring even in the IHD regime. Unfortunately, these arguments do not suffice for a full quantitative description of such phenomenon. For instance, note that in Fig. 7(a) it does not occur for $\alpha = 1$ and, moreover, is stronger for $\alpha = 0.1$ than for $\alpha = 0.05$.

Now the restriction of a fixed field amplitude is lifted. Fig. 8 presents results similar to those of Fig. 7, but for different values of h_0, with fixed $\sigma = 10$, $\alpha = 0.1$ and $\psi = 45°$. The circles in Fig. 8(a) denote the LRT results which, as can be seen, agrees precisely with $h_0 = 0.01$. Note that such exceptional correspondence strongly endorses the numerical accuracy of this method. As can be seen, up to $h_0 = 0.1$ only slight deviations from the linear behavior are observed. Moreover, a clear transition takes place between $h_0 = 0.1$ and 0.2, with the latter presenting the characteristic oscillations pertaining to non-linear resonance phenomena. Increasing the field further yields larger deviations and an increasingly more irregular response, which is also visibly quite unpredictable. Also note that these results are in complete agreement with those of Refs. 23 and 24. An important conclusion extracted from this analysis is that fields as small as $\sim$20% of the Stoner and Wolfarth field are already capable of exciting resonant hysteresis loops. This is quite relevant when one considers experimental systems, in which large magnetic fields are not easily achieved under high-frequency excitations.

VI. RANDOMLY ORIENTED ENSEMBLES

Systems with randomly oriented anisotropy axes may be computed by appropriately averaging loops for different values of ψ (steps of 2°were used). Results for fixed $\sigma = 10$ and varying α are shown in Fig. 9. The temperature dependence is treated in Fig. 10, which presents loops for different values of σ, with $\alpha = 1$ (dashed lines) and $\alpha = 0.05$ (solid lines). Such calculations are important because they give a more realistic description of real systems. In fact, the most relevant conclusion drawn from Figs. 9 and 10 is precisely that resonant hysteresis remain present, thus making it prone to experimental analysis. As for Fig. 9, the following similarities with previously presented results are worth noting: (i) shape changes begin to take place above $\omega\tau_0 = 0.1$, with forms that are clearly peculiar of the LD regime; (ii) a strong diminution of the loop height when α is small appears after $\omega\tau_0 = 0.2$; (iii) at $\omega\tau_0 = 0.55$ the loop apex is bent up; and (iv) after the ATF all curves turn into quasi-ellipsoids but only those in the LD regime become out-of-phase.

In Fig. 10 it is possible to see that the distinct temperature dependence of the LD curves, that was discussed in Sec. IV and Fig. 4, also remain in randomly oriented ensembles; that is, as ω approaches ω_R the loops become practically independent of σ but, afterward, the dependence returns. Two very important consequences follow. First, since $\sigma \propto 1/T$, this shows that RH loops are not artifacts of low temperature environments and may in fact be detected at any temperature, even in the superparamagnetic regime. Conversely, for fixed T, $\sigma \propto v$, the particle's volume. This implies that RH loops have only but a weak dependence on the particle size, a fact of considerable importance in view of the intrinsic size distributions present in any real system.

Also note that the results of Fig. 10 provide a way to measure the temperature dependence of the damping. For instance, one may first locate the RH region by finding loops that have distinct shapes. Then, on measuring curves for different temperatures, any changes observed are guaranteed not to have come from the change in T, but from that in $\alpha(T)$. Such experiments are quite relevant, both from the academic and technological standpoints. In Refs. 25 and 29, a method based on linear susceptibility was proposed that allowed α to be determined quantitatively by fitting the model to the experimental data. The present approach is clearly not as sophisticated, being limited to a qualitative analysis only.

Finally, attention is called to the interesting fact that in low frequencies [Fig. 10(a)] the area increases with decreasing α. This was also observed in Figs. 5(a) and 5(b). Although being quite subtle for $\sigma = 10$, Fig. 10(a) shows that it can become significant at the superparamagnetic regime ($\sigma = 2$; red curves) where, for instance, the coercivity for $\alpha = 0.05$ is seen to be nearly three times larger than for $\alpha = 1$. To interpret this, two arguments are necessary. The first, already discussed, is that low damping implies a longer response time. The second, required to explain the temperature dependence, is that the precession actually takes place around the total field, which includes the thermal contribution [$\mathbf{H}_{\rm th}$; cf. Eq. (1)]. The random nature of this noise-induced precession may hamper the magnetic response, thus also increasing the area.

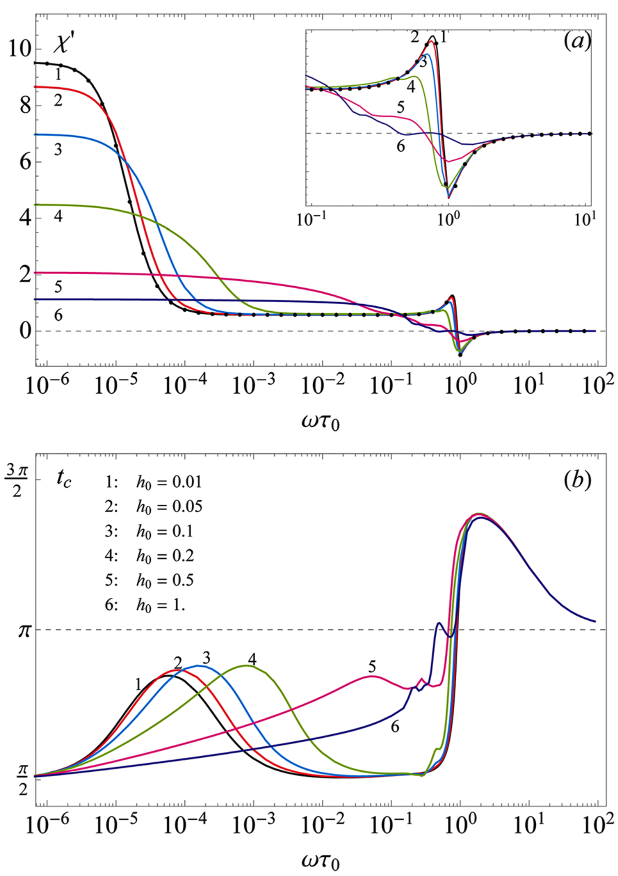

FIG. 8. (Color online) Parameters obtained from the hysteresis loops as a function of frequency for different values of h_0, with fixed $\sigma = 10$, $\alpha = 0.1$, and $\psi = 45°$. (a) Real part of the average susceptibility, Eq. (13); (inset) magnification of the FMR region. Circles denote the LRT results. (b) Coercive time.

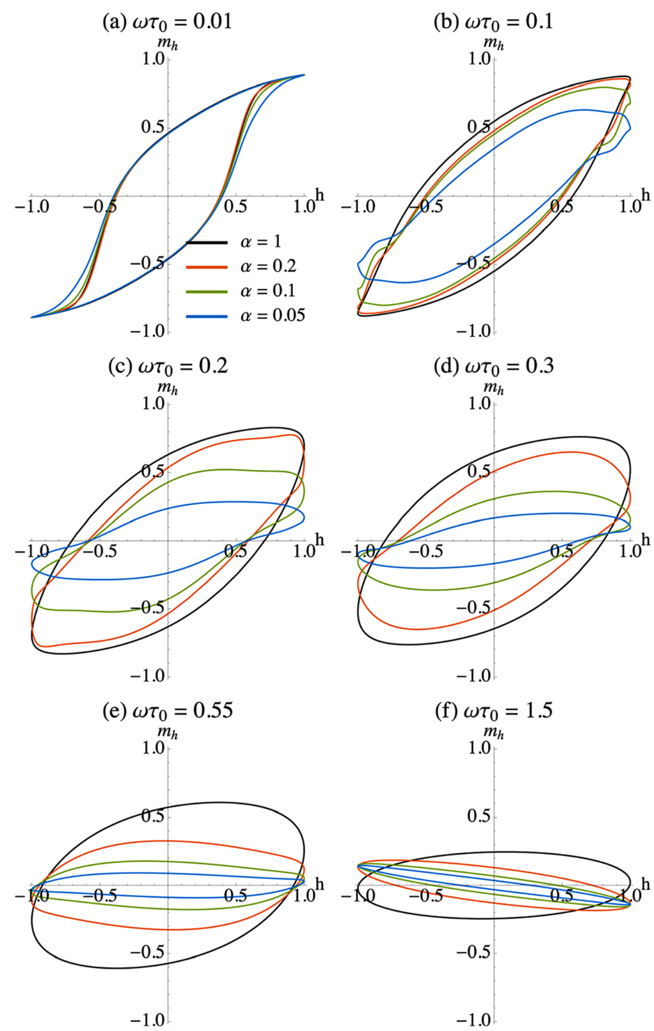

FIG. 9. (Color online) Hysteresis loops for a randomly oriented particle ensemble, with fixed $\sigma = 10$ and $h_0 = 1$.

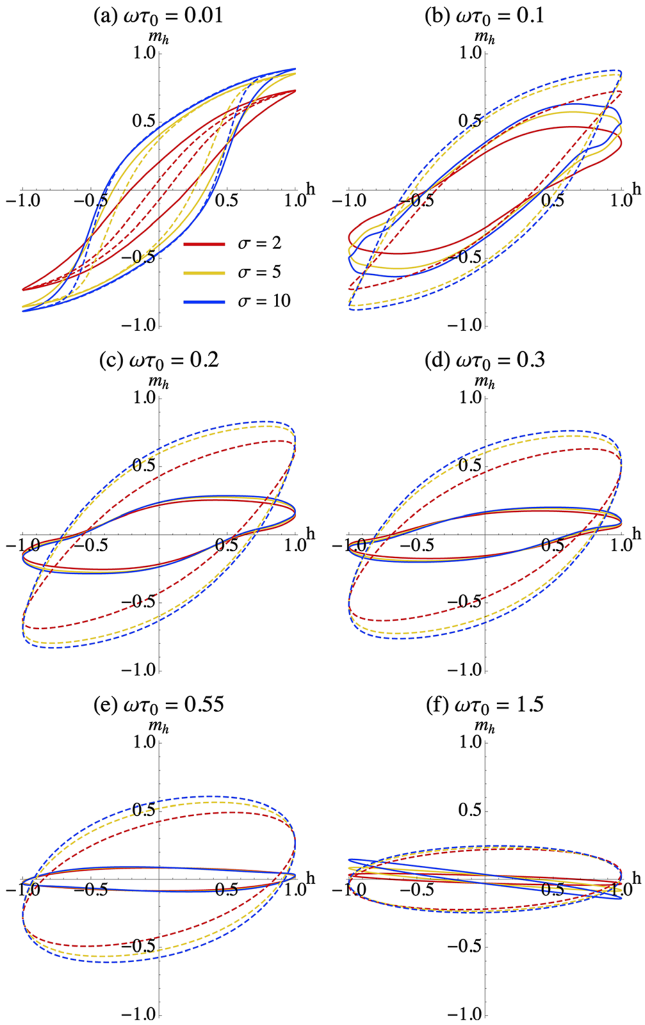

FIG. 10. (Color online) Hysteresis loops for a randomly oriented particle ensemble for different values of σ and ω, with $\alpha = 1$ (dashed lines) and $\alpha = 0.05$ (solid lines).

VII. DISCUSSION

The primary goal of this paper is to show that the magnetization damping—which is seldom included in numerical investigations of dynamic hysteresis in single domain particles—has indeed a paramount influence on the magnetic response of the system. This is particularly more so for $\omega\tau_0 \geq 0.1$, where novel effects were observed. They include, among others, the appearance of unusual and unpredictable shapes and a strong reduction of the average loop height. In fact, the magnetic behavior in this region may be deemed as unstable, with the response being sensitive to all parameters. Notwithstanding, it is remarkable that several key aspects remain in randomly oriented ensembles, as shown in Sec. VI. Moreover, in this frequency region the response is weakly dependent on the stability parameter $\sigma = Kv/k_BT$, which is a consequence of the combined influence of resonant excitations and a strong field amplitude (cf. Fig. 4 or Fig. 10). This shows that, on the one hand, this phenomenon should not be restricted to low temperatures and, on the other hand, it will not be smeared out in poly-disperse particle assemblies, which is always the case in real systems. Thus, these assertions combined allow us to conclude that resonant hysteresis loops are in fact liable for experimental analysis. Finally, the author would like to stress once more that, even though most of the analysis has focused on a fixed field amplitude of $h_0 = 1$, the results of Fig. 8 show quite clearly that resonant hysteresis loops can be excited with fields well below the Stoner and Wolfarth field, $H_A = 2K/M_s$.

As one might expect, these results differ markedly from simple models such as that of Stoner and Wolfarth where neither frequency nor temperature are considered. At low and intermediate frequencies, a better agreement is found with respect to the rate equation method of Ref. 15 and the IHD approximation of Ref. 14. This confirms the predictions that the low frequency dynamics are not strongly influenced by the damping. It is worth mentioning, however, that there exists an influence nonetheless which, albeit small, is measurable and extends throughout the entire frequency spectrum (cf. Fig. 7). On the other hand, above $\omega\tau_0 \simeq 0.1$ these results are entirely novel and differ markedly from all these previous studies.

Results for the non-linear response for arbitrary values of α have been recently reported in Refs. 23 and 24, which focused on the behavior of $\chi_1(\omega)$, the first term in the Fourier series expansion of the magnetic response. As already mentioned, because of the orthogonality of the harmonic functions, this agrees with the definition of $\chi(\omega)$ as the average susceptibility per cycle. In terms of these quantities, the present results agree consistently with theirs, as one would expect given that both stem from the very same model (note that the solution methods are different; see the following). Attention is called, however, to the fact that in those papers the frequency was normalized by the Néel relaxation time, $\tau_N = \tau_0\sigma(1+\alpha^2)/\alpha$, which depends explicitly on the damping. When comparing results for different values of α, such a choice gives the possibly misleading impression that the FMR occurs at different frequencies; as discussed in the present paper, this is certainly not the case (cf. the inset in Fig. 3).

Now discussed is the numerical approach employed in this paper and how it compares with other methods usually found in the literature. Although certainly not new, this approach is seldom used in this type of stochastic problem, with the method of choice being usually MCF,[18,19] whose convergence rate and accuracy are both noteworthy. Notwithstanding, in terms of computational efficiency, this approach is by no means inferior. This follows from the remarkable efficiency of libraries, such as SUNDIALS,[17] in treating systems of ODEs with sparse Jacobian matrixes, as in the present case. However, an important aspect of this method is that the average computational time depends heavily on the relative magnitude of the terms appearing in Eq. (10). This is a consequence of the adaptive step size used to maintain the solution within the prescribed error tolerances. The damping, in particular, may vary over several orders of magnitude and is therefore the primary factor in the convergence of the calculations. Indeed, the increase in computational time from, say, $\alpha = 1$ to $\alpha = 0.01$ is well over 20-fold. This research was unaware of the scaling of MCF methods with α but, from the range of results usually presented in the literature,[22–25] this seems like a clear disadvantage of this current method.

There is, however, another difference between the two that is of particular importance, which is the simplicity of the current approach. There are several obvious advantages in using the hierarchy of differential recurrence relations—as compared to the direct solution of the Langevin equation—that justify the analytical effort involved in deriving it. From there on, however, it is also necessary to implement it, so as to be used for computational purposes, and it is in this sense that both methods diverge contrastingly. If one is interested only in the linear response, the MCF method requires some effort in arranging matrixes, which is not markedly different from this method. Thus, given it is superior convergence rate, the MCF will unquestionably be superior. However, for the nonlinear response a further expansion in Fourier series is required, which gives a different hierarchy, now notably more complex. This in turn requires a complicated arranging of supermatrixes in order to cast the system in a numerically solvable form. Moreover, this is only possible for harmonic fields, which limits considerably it is use in other applications as, for instance, pulsed magnetic fields. In this approach there are no intermediate steps from the hierarchy to the numerical solution since, after truncating Eq. (10), the ODE system desired is already obtained. It also follows that the procedure is independent of the form of the applied field. Indeed, any parameter appearing in Eq. (10) may be taken as time-dependent if desired. Conversely, one possible disadvantage of this method is the need to eliminate transients, a feature which is entirely absent in the MCF approach. However, as discussed, the computational burden of such is quite low and, moreover, an analysis of transients may actually be of value in certain physical situations.

By comparing these calculations with a variety of other methods (SLL, LRT, and IHD regime) the accuracy of the proposed method was able to be scrutinized. Note, in particular the exceptional agreement with the SLL calculations, as shown in Figs. 2 and 6. This is quite important given that the latter is the only choice available when one wishes to consider interacting particles. In a recent paper[30] it was shown that in magnetic relaxation the initial conditions are paramount for both methods to agree. These results which, on the other hand, must be entirely independent of transients, also corroborate their equivalence.

It is straightforward to translate the results presented in this paper to real systems. Take for instance the popular material maghemite. Using $K \simeq 10^5\,\text{erg/cm}^3$ and $M_s \simeq 500\,\text{G}$ one arrives at $H_A \simeq 400\,\text{G}$ which, as usual, gives $\tau_0 \simeq 10^{-10}\text{s}$. Therefore, the lowest and highest frequencies employed were respectively $\omega \sim 10^2\,\text{Hz}$ and $\omega \sim 10^{12}\,\text{Hz}$. Notice that the latter is still below the Nyquist frequency, which is $\sim 10^{13}$ Hz, and in principle justifies the correctness of the approximation of a white noise thermal field[16] [Eq. (6)]. The values of h_0 studied in Sec. V, Fig. 8, correspond directly to fractions of H_A. Hence, above $\sim$40 G (i.e., $h_0 = 0.1$), one should already observe strong deviations from the linear behavior. Finally, assuming particles with 4 nm radius $Kv/k_B \simeq 200\,K$ is obtained, which immediately allows one to convert between σ and T through the relation $T = (Kv/k_B)\sigma^{-1} \approx 200 \times \sigma^{-1}$. Thus, $\sigma = 10$, 5, and 2 correspond to 20, 40, and 100 K, respectively.

VIII. CONCLUSIONS

In summary, the influence of the magnetization damping on dynamic hysteresis loops in single-domain particles has been discussed in detail. The system was assumed to have uniaxial anisotropy and calculations were performed, which are free of any approximations, except those already implied by the Néel-Brown theory. The proposed numerical procedure has shown to be of remarkable efficiency and simplicity, being also readily applicable in a variety of other problems in magnetism and stochastic processes. These results indicate that above a frequency of $\sim$1/10 of the resonance frequency the magnetization damping influences drastically the magnetic behavior, leading to novel and interesting effects.

ACKNOWLEDGMENTS

The author acknowledges A. D. Santos, F. L. Maximino, and G. F. Oliveira for stimulating discussions. This work was supported by the Brazilian funding agency FAPESP.

APPENDIX A: DIFFERENTIAL RECURRENCE RELATIONS

In order to go from Eq. (9) to Eq. (10), first write the former in spherical coordinates. Since $f(\mathbf{m}) = Y_{l,m}(\theta,\ \phi)$, $\partial f/\partial \mathbf{m} = \nabla Y_{l,m}(\theta,\ \phi)$ where

$$\nabla Y_{l,m} = \frac{\partial Y_{l,m}}{\partial \theta}\hat{\theta} + \frac{1}{\sin\theta}\frac{\partial Y_{l,m}}{\partial \phi}\hat{\phi} = \hat{\theta}\left[-(l+1)\frac{\cos\theta}{\sin\theta}Y_{l,m} + \frac{1}{\sin\theta}\sqrt{\frac{2l+1}{2l+3}}\sqrt{(l+1)^2 - m^2}Y_{l+1,m}\right] + \hat{\phi}\left(\frac{im}{\sin\theta}Y_{l,m}\right). \tag{A1}$$

Here, $\hat{\theta}$ and $\hat{\phi}$ are the unit vectors in the polar and azimuthal directions respectively. If the effective field is written as $\mathbf{h}_e = h_r\hat{r} + h_\theta\hat{\theta} + h_\varphi\hat{\phi}$, then on noting that $\mathbf{m} \equiv \hat{r}$ (the radial unit vector), Eq. (9) becomes

$$(1+\alpha^2)\tau_0\frac{dY_{l,m}}{dt} - \left[(\alpha h_\theta + h_\phi)\hat{\theta} + (\alpha h_\phi + h_\theta)\hat{\phi}\right] \cdot \left[\frac{\partial Y_{l,m}}{\partial\theta}\hat{\theta} + \frac{1}{\sin\theta}\frac{\partial Y_{l,m}}{\partial\phi}\hat{\phi}\right] + \frac{\alpha}{2\sigma}l(l+1)Y_{l,m}, \tag{A2}$$

where

$$h_\theta = h_0(-\gamma_z\sin\theta + \gamma_x\cos\theta\cos\phi) - \sin\theta\cos\theta$$
$$h_\phi = -h_0\gamma_x\sin\phi.$$

After expanding the dot product in Eq. (A2) one is left with products of the trigonometric functions and the $Y_{l,m}$. To write these as linear combinations of spherical harmonics it is necessary to make use of the following formula:

$$Y_{l,m}Y_{l,m_1} = \sqrt{\frac{(2l+1)(2l_1+1)}{4\pi}}\sum_{l_2=|l-l_1|}^{l+l_1}\frac{C^{l_2,0}_{l,0,l_1,0}C^{l_2,m+m_1}_{l,m,l_1,m_1}}{\sqrt{2l_2+1}}Y_{l_2,m+m_1},$$

where C are the Clebsch-Gordan coefficients. Fortunately, only three relations suffice,

$$\cos\theta Y_{l,m} = \sqrt{\frac{l^2-m^2}{4l^2-1}}Y_{l-1,m} + \sqrt{\frac{(l+1)^2-m^2}{(2l+1)(2l+3)}}Y_{l+1,m}$$

$$\cos^2\theta Y_{l,m} = \sqrt{\frac{(l^2-m^2)\left[(l-1)^2-m^2\right]}{(2l-3)(2l-1)^2(2l+1)}}Y_{l-2,m} + \sqrt{\frac{\left[(l+1)^2-m^2\right]\left[(l+2)^2-m^2\right]}{(2l-1)(2l+3)^2(2l+5)}}Y_{l+2,m} + \left[\frac{2}{3}\frac{l(l+1)}{(2l-1)}\right]$$

$$\sqrt{\frac{8\pi}{3}}Y_{1,\pm1}Y_{l,m} = \sqrt{\frac{(l\pm m+1)(l\pm m+2)}{(2l+1)(2l+3)}}Y_{l+1,m\pm1} - \sqrt{\frac{(l\mp m-1)(l\mp m)}{(2l-1)(2l+1)}}Y_{l-1,m\pm1}.$$

It is also necessary to use the last equation with $Y_{1,\pm1}$ in the denominator, which can be written as

$$\frac{Y_{l,m}}{Y_{1,\pm1}} = \sqrt{\frac{8\pi}{3}\frac{(2l-1)(2l+1)}{(l\pm m)(l\pm m-1)}}Y_{l-1,m\mp1} + \sqrt{\frac{(2l-1)(l\mp m)(l\mp m-1)}{(2l-3)(l\pm m)(l\pm m-1)}}\frac{Y_{l-2,m}}{Y_{1,\pm1}}.$$

With these equations one is able to write Eq. (A2) entirely as linear combinations of the $Y_{l,m}$ and hence arrive at Eq. (10).

APPENDIX B: LINEAR RESPONSE THEORY

The main result from the LRT is that $\chi(\omega)$ may be computed as the one-sided Fourier transform of the magnetic relaxation autocorrelation function $m_r(t)$, calculated in the absence of an external field. Namely

$$\frac{\chi(\omega)}{\chi(0)} = 1 - i\omega\int_0^\infty m_r(t)e^{-i\omega t}dt. \tag{B1}$$

The relaxation assumes that a small static field ($h \ll 1$) has been applied for an infinitely long time up to $t=0$ where it was abruptly shut off. Whence, $m_r(t)$ is easily calculated from the ODE system,[11] by defining $\tilde{\mathbb{X}} = \mathbb{X} - \left(\mathscr{F}^{-1}\mathbb{U}\right)_{h=0}$. It then follows that $\dot{\tilde{\mathbb{X}}} = \mathscr{F}_{h=0}\tilde{\mathbb{X}}$, which corresponds to a system of linear ODEs with constant coefficients, whose solution may immediately be written as

$$\tilde{\mathbb{X}}(t) = \sum_{k=1}^{N} a_k \mathbf{g}_k e^{p_k t}. \tag{B2}$$

Here the p_k are the eigenvalues of $\mathscr{F}$ and $\mathbf{g}_k$ its corresponding eigenvectors. The a_k are constants to be determined from the initial condition vector $\tilde{\mathbb{X}}_0$. This in turn is also obtained from Eq. (11) by solving the linear system

$$\tilde{\mathbb{X}}_0 = \lim_{h\to 0}\left[\frac{\left(\mathscr{F}^{-1}\mathbb{U}\right)_{h\neq 0} - \left(\mathscr{F}^{-1}\mathbb{U}\right)_{h=0}}{h}\right]. \tag{B3}$$

Although other methods such as, e.g., using the equilibrium partition function, can be used to determine the initial conditions, this equation has the merit of being readily available and hence easily calculable.

One may prove that the eigenvalues arising from the Fokker-Planck equations are always in the open left half-plane[19] from where it follows that $\mathscr{F}$ must always be stable. The author writes $p_k = -\lambda_k + i\mu_k$ with $\lambda_k > 0$. If $\alpha \to \infty$, then $\mu_k \equiv 0$ and only exponentially decaying relaxation mechanisms are possible. If not, then the eigenvalues of $\mathscr{F}$ will appear as complex conjugate pairs and oscillatory solutions will surface. After finding the a_k's one may use an equation similar to Eq. (12) to write the desired relaxation autocorrelation function as

$$m_r(t) = \sum_k e^{-\lambda_k t}\left\{c_k^{(1)}\cos\mu_k t + c_k^{(2)}\sin\mu_k t\right\}, \tag{B4}$$

where $c_k^{(1)}$ and $c_k^{(2)}$ are constants and the sum is taken over distinct eigenvalues. Finally, upon calculating the integral in Eq. (B1) the author arrives at

$$\frac{\chi(\omega)}{\chi(0)} = 1 - i\omega\sum_k \frac{c_k^{(1)}(\lambda_k + i\omega) + c_k^{(2)}\mu_k}{\mu_k^2 + (\lambda_k + i\omega)^2}, \tag{B5}$$

which gives $\chi(\omega)$ for arbitrary ω.

[1]S. Sun, C. Murray, D. Weller, L. Folks, and A. Moser, Sciences (N.Y.) **287**, 1989 (2000).
[2]Q. A. Pankhurst, N. K. T. Thanh, S. K. Jones, and J. Dobson, J. Phys. D **42**, 224001 (2009).
[3]C. Bean and I. Jacobs, J. Appl. Phys. **27**, 1448 (1956).
[4]L. Néel, Ann. Géophys. **5**, 99 (1949).
[5]P. Gambardella, S. Rusponi, M. Veronese, S. S. Dhesi, C. Grazioli, A. Dallmeyer, I. Cabria, R. Zeller, P. H. Dederichs, K. Kern, C. Carbone, and H. Brune, Sciences (N.Y.) **300**, 1130 (2003).
[6]J. Rantschler, R. McMichael, A. Castillo, A. Shapiro, W. Egelhoff, Jr., B. Maranville, D. Pulugurtha, A. Chen, and L. Connors, J. Appl. Phys. **101**, 033911 (2007).
[7]G. Woltersdorf, M. Kiessling, G. Meyer, J.-U. Thiele, and C. Back, Phys. Rev. Lett. **102**, 257602 (2009).
[8]J. L. Dormann, F. Lucari, F. D'Orazio, E. Tronc, P. Prené, J. P. Jolivet, D. Fiorani, R. Cherkaoui, and M. Noguès, Phys. Rev. B **53**, 291 (1996).
[9]H. Ebert, S. Mankovsky, D. Ködderitzsch, and P. Kelly, Phys. Rev. Lett. **107**, 066603 (2011).
[10]A. Brataas, Y. Tserkovnyak, and G. E. W. Bauer, Phys. Rev. Lett. **101**, 037207 (2008).
[11]J. Carrey, B. Mehdaoui, and M. Respaud, J. Appl. Phys. **109**, 083921 (2011).
[12]P. M. Déjardin, Y. P. Kalmykov, B. E. Kashevsky, H. El Mrabti, I. S. Poperechny, Y. L. Raikher, and S. V. Titov, J. Appl. Phys. **107**, 073914 (2010).
[13]G. T. Landi, J. Magn. Magn. Mater. **324**, 466 (2011).
[14]I. Poperechny, Y. Raikher, and V. I. Stepanov, Phys. Rev. B **82**, 174423 (2010).
[15]N. A. Usov, J. Appl. Phys. **107**, 123909 (2010).
[16]W. Brown, Phys. Rev. **130**, 1677 (1963).

[17]A. C. Hindmarsh, P. N. Brown, K. E. Grant, S. L. Lee, R. Serban, D. A. N. E. Shumaker, and C. S. Woodward, ACM Trans. Math. Softw. **31**, 363 (2005).
[18]W. Coffey, Y. P. Kalmykov, and J. Waldron, *The Langevin Equation. With Applications to Stochastic Problems in Physics, Chemistry and Electrical Engineering*, 2nd ed. (World Scientific, Singapore, 2004), p. 678.
[19]H. Risken, *The Fokker-Planck Equation*, 2nd ed. (Springer, Berlin, 1989).
[20]E. Stoner and E. Wohlfarth, Philos. Trans. R. Soc. London, Ser. A **240**, 599 (1948).
[21]M. Abramowitz and I. Stegun, *Handbook of Mathematical Functions* (Dover, New York, 1964).
[22]W. Coffey, D. S. F. Crothers, J. L. Dormann, L. J. Geoghegan, and E. C. Kennedy, Phys. Rev. B **58**, 3249 (1998).
[23]H. E. Mrabti, S. V. Titov, P.-M. Dejardin, and Y. P. Kalmykov, J. Appl. Phys. **110**, 023901 (2011).
[24]S. Titov, P.-M. Déjardin, H. El Mrabti, and Y. Kalmykov, Phys. Rev. B **82**, 100413 (2010).
[25]W. Coffey, D. Crothers, Y. Kalmykov, and S. Titov, Phys. Rev. B **64**, 012411 (2001).
[26]P. E. Kloeden and E. Platen, *Numerical Solution of Stochastic Differential Equations*, 2nd ed. (Springer, Berlin, 1995).
[27]J. L. Garcia-Palacios and F. Lázaro, Phys. Rev. B **58**, 14937 (1998).
[28]A. Smirnov and A. Pankratov, Phys. Rev. B **82**, 132405 (2010).
[29]J. L. Garcia-Palacios and P. Svedlindh, Phys. Rev. Lett. **85**, 3724 (2000).
[30]Y. Kalmykov, W. Coffey, U. Atxitia, O. Chubykalo-Fesenko, P.-M. Déjardin, and R. Chantrell, Phys. Rev. B **82**, 024412 (2010).